

GRISTORM: GRID-BASED VARIABLE SOURCE AREA STORM RUNOFF MODEL

S. J. Kim, T. S. Steenhuis

ABSTRACT. A grid-based storm runoff model in a variable source area is described. This model predicts temporal variations and spatial distributions of subsurface flow-saturation overland flow with various shallow soil depths. The model uses ASCII-formatted map data supported by the GRASS Geographic Information Systems (GIS) and generates distributed results such as discharge, flow depth, and soil moisture in overland flow areas. The model uses a single overland flowpath algorithm and simulates surface and/or subsurface water depth at each grid element for a given time increment. A combined surface-subsurface kinematic modeling approach was used to simulate surface and subsurface flow. The model was applied to a 170 ha watershed located in New York State. Predicted flows from six summer storm events in 1994 were compared with observed flows at the watershed outlet. The initial soil moisture conditions for the storm events were based on calibrated values from Frankenberger's Soil Moisture Routing (SMR) model and were adjusted to include soil moisture variations within a day. The average Nash-Sutcliffe efficiency for predicting runoff at the watershed outlet using calibrated parameters for three storm events was 0.72. The initial soil moisture distribution proved to be the most sensitive parameter affecting stream flow at the watershed outlet and required calibration to obtain reasonable results. The second most sensitive parameter was Manning's roughness coefficient for stream and overland areas. It affected the time and magnitude of peak stream flow. Results showing temporal variations and spatial distributions of overland flow areas were presented using GRASS. According to the results showing the spatial effect with differing grid element sizes, the model behavior was also sensitive to DEM grid resolution.

Keywords. Modeling, Grid-based, Storm runoff, Variable source area, GRASS, Geographic Information Systems.

A hydrologic model that predicts surface and subsurface flows and their flowpaths to the stream requires the incorporation of throughflow processes in the GIS (Geographic Information Systems) framework. Many catchment models have been proposed, but few treat throughflow effectively. Several distributed physically based catchment models exist, such as SHE (Abbott et al., 1986), MIKE SHE (Refsgaard and Storm, 1995), IHDM (Beven et al., 1987), and THALES (Grayson et al., 1992).

The source area for overland flow in a watershed shrinks and expands in response to rainfall in humid, well-vegetated areas (Tischendorf, 1969; Dunne and Black, 1970; Hewlett and Nutter, 1970). The source area may be regarded as an expansion of the perennial channel system into zones of low storage capacity fed from below by subsurface stormflow and from above by rainfall. During rainless periods, streams are fed largely by moisture migrating slowly downslope under conditions of unsaturated flow (Kirkby, 1978). As Dunne and Black (1970) point out, the source area generates overland

flow, while the remainder of the watershed acts mainly as a reservoir during storms to provide baseflow and to maintain the wet areas that will produce subsequent storm runoff. This is especially true for well-vegetated watersheds in the northeastern United States, in which shallow and sloping soils predominate and for which the hydraulic conductivity of soils exceeds rainfall intensity by several fold (Kuo et al., 1999). A GIS can help to apportion storm runoff between the various flowpaths associated with source areas on slopes.

Recently, several researchers have attempted to model the rainfall-runoff processes with GIS. GIS has proven to be an efficient tool for spatial analyses by visualizing the results of hydrologic and water quality modeling. Allen (1987) developed SWHAM (Small Watershed Hydrologic Analysis Model) using a GIS. This overland flow model is composed of a one-dimensional groundwater hydrologic model and a stream flow model. Input data were extracted from soil, land use/cover, and contour maps. Stuebe and Johnston (1990) applied GIS to all phases of the SCS (Soil Conservation Service) modeling processes, including watershed delineation and runoff routing, to estimate the outlet runoff volume. Stuebe and Johnston's work demonstrated the use of GRASS to estimate runoff using the SCS runoff Curve Number Model. Famiglietti (1992) used grid data extracted from a GIS to develop a model with grid-based water balance and flow equations. Zollweg (1994) developed SMoRMod (Soil Moisture-based Runoff Model) using a series of GRASS commands. The model is grid-based and composed of a daily soil moisture balance and sub-routines that calculate runoff generation and transport at 30-minute intervals. The initial conditions for the runoff generation are

Article was submitted for review in August 2000; approved for publication by the Soil & Water Division of ASAE in April 2001.

The authors are **Seong J. Kim**, *ASAE Member Engineer*, Assistant Professor, Department of Biological Systems Engineering, Konkuk University, Seoul, Korea; and **Tammo S. Steenhuis**, *ASAE Member Engineer*, Professor, Department of Agricultural and Biological Engineering, Cornell University, Ithaca, New York. **Corresponding author:** Seong J. Kim, Department of Biological Systems Engineering, Konkuk University, Seoul 143-701, Korea; phone: +82-2-450-3749; fax: +82-2-444-0186; e-mail: kimsj@konkuk.ac.kr.

provided by the daily soil moisture balance. However, the model has a tendency to over- or under-predict the recession part of hydrographs. Savabi et al. (1995) used GRASS to obtain the WEPP (Water Erosion Prediction Project) model's input parameters. Frankenberger (1996) and Frankenberger et al. (1999) modified Zollweg's GIS-Based Variable Source Area Model using GRASS. The model, written in UNIX-shell script, predicts daily soil moisture and runoff based on a water balance for shallow soils.

It is evident that during the past decade, distributed modeling of surface and subsurface hydrology has become computational, primarily because of the capability of GIS to handle spatial data. Some studies have been conducted by coupling GIS with distributed models within GIS software, called tight coupling (Stuart and Stocks, 1993). This is an embedded system where the GIS and models rely on a single data manager. It makes the processes clear for the user to understand and modify for different conditions. On the other hand, extensive progress has been made in managing distributed models outside GIS, referred to as loose coupling (Goodchild, 1993; Nyerges, 1993). This makes the model flexible and portable to another GIS software.

In this article, a grid-based subsurface and saturation overland/stream flow generation procedure is described. This approach predicts the temporal variation and spatial distribution of overland flow depth, discharge, and soil moisture during a storm event. The applicability of the procedure and its modification of the original surface and subsurface kinematic modeling approach by Takasao and Shiiba (1988) are also described. The model, coded in UNIX-C language, runs in GRASS (U.S. Army CERL, 1993) and uses regular gridded data such as elevation, stream, land use, and soil information. The data used for this study were previously developed and described in Frankenberger (1996). The spatial results are displayed in GRASS.

MODEL DESCRIPTION

SATURATION OVERLAND/STREAM FLOW AND SUBSURFACE FLOW MODEL

Storm runoff in the northeastern United States, where the land surface is well vegetated, originates mainly from saturated areas (Dunne and Black, 1970). Saturated areas often form where lateral subsurface flows converge, slopes change, or where depth to the restricting layer decreases (Frankenberger, 1996). The amount of storm runoff is directly related to the magnitude of the saturated areas.

In order to model the formation of variable source areas, we adopted the combined surface-subsurface kinematic modeling approach (Takasao and Shiiba, 1988). The continuity equation applied to each grid element can be written as:

$$\frac{\partial A}{\partial t} + \frac{\partial Q}{\partial \ell} = \frac{rA_c}{L_c} + \frac{Q_\ell}{L_\ell} \quad (1)$$

where

- A = flow area (m²)
- Q = discharge (m³/sec)
- r = rainfall intensity (m/sec)
- A_c = grid element area of grid element c (m²)
- L_c = flow distance through the grid element c (m)

Q_ℓ = lateral discharge (m³/sec)

L_ℓ = lateral flow length (m)

t = time (sec)

ℓ = length (m).

The flow areas for subsurface and saturation overland/stream flow are:

$$A = W_c \times EP_c \times H, 0 \leq H \leq D_c \quad (2)$$

$$A = W_c \times EP_c \times D_c + A_f, H > D_c \quad (3)$$

$$A_f = W_c \times (H - D_c) \quad (4)$$

where

W_c = grid element width orthogonal to streamline (m)

EP_c = total porosity minus field capacity (m³/m³)

D_c = soil depth above the impeding layer (m)

H = flow depth above the impeding layer (m)

A_f = overland flow area (m²).

The resistance equation for subsurface flow, and the kinematic wave equation for saturation overland/stream flow are obtained by Darcy and Manning equations, respectively:

$$Q = K_e \times \frac{A}{EP_c} \sin(\beta), 0 \leq H \leq D_c \\ = W_c \times H \times K_e \sin(\beta) \quad (5)$$

$$Q = W_c \times D_c \times K_e \sin(\beta) + \alpha A_f^m, H > D_c \quad (6)$$

where

K_e = saturated hydraulic conductivity (m/sec)

β = grid element slope (degree)

$m = 5/3$ for overland flow as shallow sheet flow ($R_h = H$) and $4/3$ for stream flow

$\alpha = n^{-1} W_c^{-2/3} \tan^{1/2} \beta$ for overland flow and $n^{-1} \gamma^{2/3} \tan^{1/2} \beta$ for stream flow

n = Manning's roughness coefficient

$\gamma = R_h A_f^{-1/2}$ (Moore and Foster, 1990; Moore and Burch, 1986)

R_h = hydraulic radius.

The schematic representation of the flow system is shown in figure 1. The finite difference form of equation 1 is expressed as:

$$A_4 + 2Q_4 \frac{\Delta t}{L_c} = A_1 - A_2 + A_3 \\ + 2Q_2 \frac{\Delta t}{L_c} + 2rA_c \frac{\Delta t}{L_c} + 2Q_\ell \frac{\Delta t}{L_c} \quad (7)$$

where

Δt = time interval

A_1, A_3 = flow area at time t at the inlet and outlet of the grid element, respectively

A_2, A_4 = flow area at time t + Δt at the inlet and outlet of the grid element, respectively

Q_2, Q_4 = discharge at time t + Δt at the inlet and outlet of the grid element, respectively.

To solve equation 7, the four-point implicit scheme developed by Brakensiek (1967) was adopted. The equation was rearranged to solve for flow depth (H), and the Newton-Raphson method (Johnson and Riess, 1982) was used to

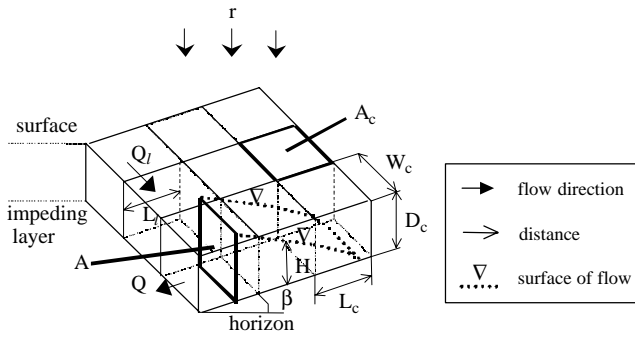


Figure 1. Schematic representation of the flow system.

calculate it at the outlet of the grid element after a given time interval.

INITIAL AND BOUNDARY FLOW DEPTH CONDITIONS OF VARIOUS SHALLOW SOIL DEPTHS

The spatial distribution of initial flow depths in a watershed can be obtained from soil information describing porosity, field capacity, and initial soil moisture conditions. The initial flow depth (H_i) for each grid element can be calculated by:

$$\begin{aligned} H_i &= D_c \frac{SM_i - F_c}{P_e - F_c}, & F_c < SM_i < P_e \\ H_i &= D_c, & SM_i \geq P_e \\ H_i &= 0, & SM_i \leq F_c \end{aligned} \quad (8)$$

where

SM_i = initial soil moisture content in grid element (m^3/m^3)

P_e = effective porosity in grid element (m^3/m^3)

F_c = field capacity in grid element (m^3/m^3).

Because each grid element has a unique flow depth value, there exist two boundary values of flow depth between the neighboring grid elements. To remove a discontinuity in flow depth, a linear interpolation is used to obtain one flow depth at each grid element boundary.

In the case of changes in soil depth between grid elements (fig. 2), the boundary flow depth can be calculated as follows, and the interpolated value at the boundary was used:

$$H_{i1}' = H_{i1} + \frac{D_{c1} - H_{i1} - (D_{c2} - H_{i2})}{2}, \quad H_{i1}' \geq D_{c1} - D_{c2} \quad (9)$$

$$H_{i1}' = D_{c1} - D_{c2}, \quad H_{i1}' < D_{c1} - D_{c2} \quad (10)$$

$$H_{i2}' = H_{i2} - (D_{c2} - D_{c1}), \quad H_{i2}' \geq D_{c1} - D_{c2} \quad (11)$$

$$H_{i2}' = 0, \quad H_{i2}' < 0 \quad (12)$$

where

H_{i1}' = interpolated flow depth of the deep grid element (m)

H_{i2}' = interpolated flow depth of the shallow grid element (m)

H_{i1} = initial flow depth of the deep grid element (m)

H_{i2} = initial flow depth of the shallow grid element (m)

D_{c1} = deep soil depth element (m)

D_{c2} = shallow soil depth element (m).

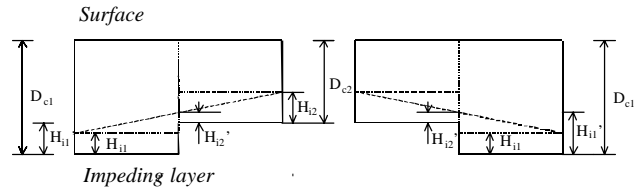


Figure 2. Interpolation of initial flow depth at grid element boundary.

At the watershed boundary, flow depth conditions at the outer boundary of the grid element are assumed zero.

OVERLAND FLOW PATTERN CLASSIFICATION AND STREAM FLOW

We can choose a 3×3 grid filter to determine flow direction. First, the flow direction from the center grid element is determined by identifying the steepest slope to the eight neighboring grid elements. The direction of steepest descent downhill, numbering 1 to 8 to the center grid element, eventually generates flow direction. Second, the subsurface/surface flow depth at the outlet of the center grid is calculated by equation 7 for a given time increment. Third, the water of the grid element flows in the steepest direction. This means that a single output flowpath is chosen, but the inflow to a grid element can come from multiple sources. To deal with multiple inlets, the eight neighboring grid elements are treated as inflow only if the flow direction number among them matches the already-determined flow direction grid. If overland flows drain into a stream, then they are treated as lateral flow to the stream.

The flow condition in a grid element can be classified into four types, and the following equations are derived from equation 7. The first type (fig. 3A) is subsurface flow at both inlet and outlet of the grid element as follows:

$$\begin{aligned} &W_c E P_c H_4 + 2W_c H_4 K_c \sin \beta \frac{\Delta t}{L_c} \\ &= W_c E P_c (H_1 - H_2 + H_3) \\ &+ 2W_c H_2 K_c \sin \beta \frac{\Delta t}{L_c} \\ &+ 2r A_c \frac{\Delta t}{L_c} + 2Q_l \frac{\Delta t}{L_c} \end{aligned} \quad (13)$$

where

H_1, H_3 = flow depth at time t at the inlet and outlet of the grid element, respectively

H_2, H_4 = flow depth at time $t + \Delta t$ at the inlet and outlet of the grid element, respectively.

The second type (fig. 3B) is saturated overland flow, that is, surface flow conditions at both inlet and outlet, as follows:

$$\begin{aligned} &W_c H_4 + 2[W_c (H_4 - D_c)]^m n^{-1} W_c^{-2/3} \tan^{-1/2} \beta \frac{\Delta t}{L_c} \\ &= W_c (H_1 - H_2 + H_3) \\ &+ 2[W_c (H_2 - D_c)]^m n^{-1} W_c^{-2/3} \tan^{-1/2} \beta \frac{\Delta t}{L_c} \\ &+ 2r A_c \frac{\Delta t}{L_c} + 2Q_l \frac{\Delta t}{L_c} \end{aligned} \quad (14)$$

The third type (fig. 3C) is a sink, that is, surface flow at the inlet and subsurface flow at the outlet. The last type (fig. 3D) is a source, that is, subsurface flow at the inlet and surface flow at the outlet. The last two cases cause a numerical divergence because of different flow conditions at the inlet and outlet of the grid element. Thus, in the third case, the flow depth at the inlet of the grid element was assumed to be equal to soil depth (D_c) and solved by equation 13. In the fourth case, the starting point of surface flow within a grid element was linearly interpolated using the inlet flow depth (H_1) and outlet grid depth (H_3) and solved by equation 14. The flow condition is checked by comparing soil depth and flow depth of the previous time step at both inlet and outlet boundaries of grid element. The stream flow is as follows:

$$\begin{aligned}
 & W_c H_4 + 2[W_c(H_4 - D_c)]^{m+1/3} n^{-1} \\
 & [W_c + 2(H_4 - D_c)]^{-2/3} \tan^{-1/2} \beta \frac{\Delta t}{L_c} \\
 = & W_c(H_1 - H_2 + H_3) + 2[W_c(H_2 - D_c)]^{m+1/3} \\
 & n^{-1} [W_c + 2(H_2 - D_c)]^{-2/3} \tan^{-1/2} \beta \frac{\Delta t}{L_c} \\
 & + 2rA_c \frac{\Delta t}{L_c} + 2Q_\ell \frac{\Delta t}{L_c} \quad (15)
 \end{aligned}$$

MODEL STRUCTURE AND IMPLEMENTATION

A schematic flow diagram of the GRISTORM model is shown in figure 4. As input data to the model, the seven GRASS regular gridded maps, consisting of elevation, stream, land use, soil type, porosity, field capacity, and initial soil moisture condition, are prepared. They are converted into ASCII-formatted map data using the GRASS command `r.out.ascii`. The model uses this data to generate discharge, flow depth, and soil moisture at each grid element outlet for a given time interval. In this study, the time step was 30 seconds, which was chosen because it is a sufficiently short interval not to exhaust all of the water in the grid element. Stream flow at the watershed outlet and ASCII-formatted discharge maps, flow depth maps, and soil moisture maps were generated for 10-minute intervals. The ASCII-formatted map data were converted into the GRASS maps using the GRASS command `r.in.ascii`.

WATERSHED, SOILS, LAND USE, AND STORM EVENTS

The model was tested in the Crowe Road watershed located in the Northern Catskill region of New York State.

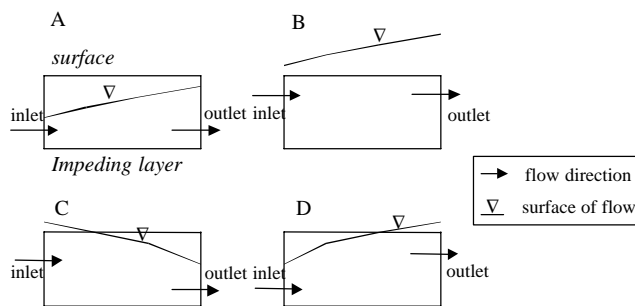


Figure 3. Four possible overland flow conditions.

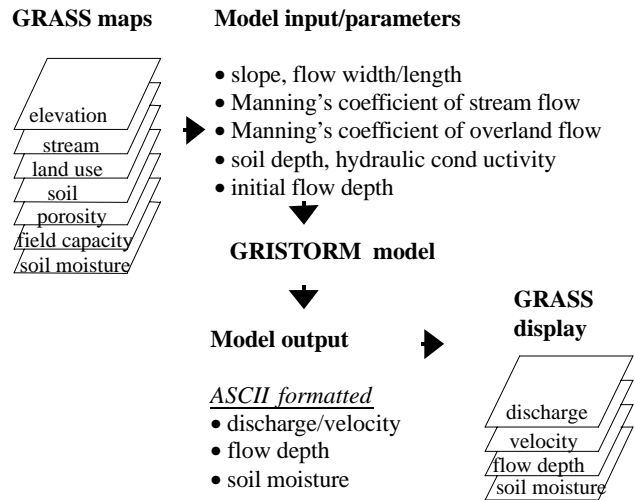


Figure 4. Schematic diagram of GRISTORM.

The watershed area is 170 ha and the elevation ranges from 580 m to 732 m. The latitude is approximately $42^\circ 30'$. The climate can be characterized as northern humid continental. The soil classification and parameters developed by Frankenberger (1996) were adopted. The watershed soils were classified as Inceptisols or Entisols, and details are shown in figure 5. The surface layer of most soils is shallow and permeable with a high percentage of rock fragments. Soil depths ranged from 25 cm to 150 cm, and the percentage of rock fragments was between 10% and 40%. The impeding layers are composed of bedrock, fragipan, and clay. The average measured saturated hydraulic conductivity in the surface layer was 2 m/day, slightly higher than the permeability range (0.4 to 1.2 m/day for all soils) of the soil survey (Frankenberger et al., 1999). Average porosity and field capacity values without rocks are 0.6 and 0.37, respectively. Land use for the watershed, as described by Frankenberger (1996), is shown in figure 6.

Precipitation and watershed outlet stream flow data were measured at 10-minute intervals by the New York State Department of Environmental Conservation. Six storm events from July and August, 1994, were chosen for model calibration and verification.

MAP DATA FROM GRASS

Elevation data were obtained from a U.S. Geological Survey quadrangle vector map of scanned 20-foot interval contour lines. Stream locations were obtained from maps supplied by the New York City Department of Environmental Protection. The soil map was rasterized to a 10 m grid size from the vector files supplied by the NRCS (Natural Resources Conservation Service). The land-use map was obtained from the NRCS and was updated from an aerial photograph and from conversations with farmers. These base maps adopted from Frankenberger (1996) have a $10\text{ m} \times 10\text{ m}$ grid element. Soil parameters were obtained from Frankenberger (1996). Daily soil moisture distribution maps generated by Frankenberger's Soil Moisture Routing (SMR) model were used as the initial soil moisture conditions for the selected storm events.

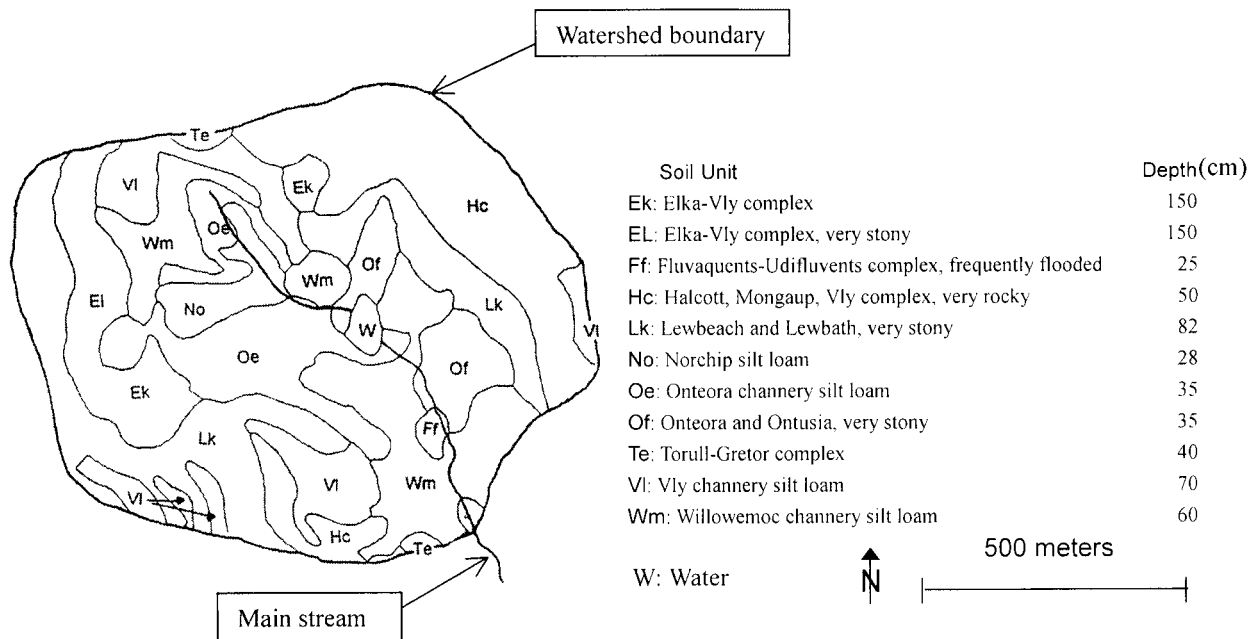


Figure 5. Soil series in the Crowe Road watershed (adopted from Frankenberger, 1996).

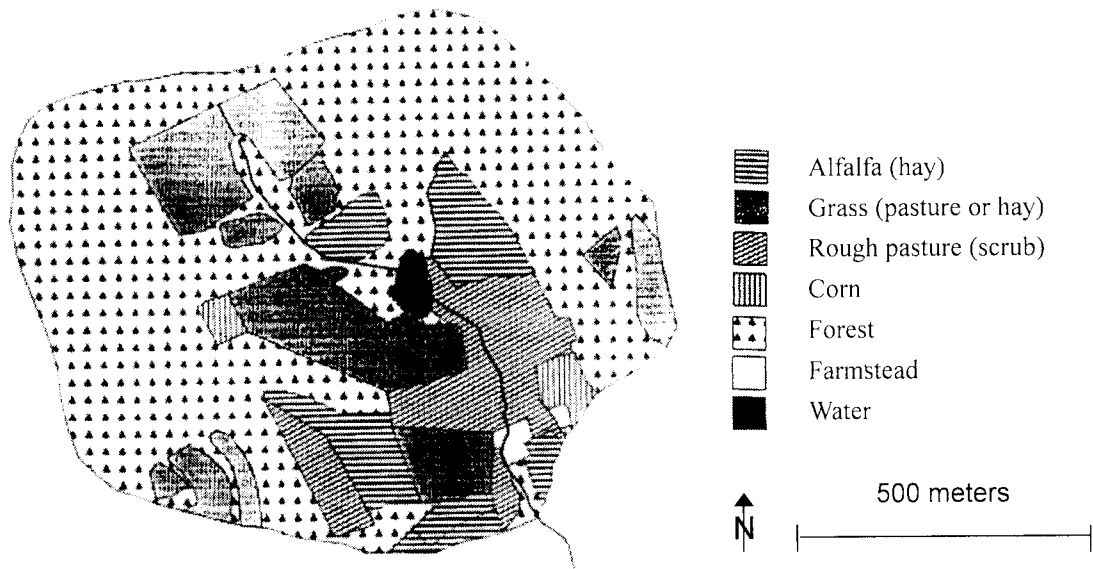


Figure 6. Land use in the Crowe Road watershed (adopted from Frankenberger, 1996).

COMPARING PREDICTED AND OBSERVED STREAMFLOW AT THE WATERSHED OUTLET *Model Calibration*

The distributed nature of models complicates proper testing and validation because the detail information provided by the model is often much greater than that measured in the catchment (Grayson et al., 1995). GRISTORM was calibrated using the stream flows at the watershed outlet, but this was an incomplete calibration due to a lack of spatial measurements of hydrologic quantities.

Frankenberger (1996) described her model results for soil moisture and found they were most accurate for the summer period, from 1 May to 15 November, 1994. The initial soil moisture conditions used in this study were based on the results of Frankenberger's Soil Moisture Routing (SMR)

model. Three storm events (2 July, 22 July, and 18 August, 1994) were selected for calibration. Table 1 shows the calibrated parameters for the three storm events. The maximum intensity and duration of the 2 July, 22 July, and 18 August storms were 38.6 mm/hr and 2.17 hours, 53.2 mm/hr and 1.17 hours, 54.8 mm/hr and 5.17 hours, respectively. The first two events had dry initial soil moisture conditions, and the last event had wet initial conditions due to rainfall on the previous day. The previous day's soil moisture distribution maps from Frankenberger's model were originally chosen as the initial soil moisture conditions for the storm events. However, the results were adjusted in this study because the simulated soil moisture distribution was the result of daily soil moisture routing that did not include adjustment for rainfall that occurred within a day.

Table 1. Summary of model calibration and its parameters.

Storm Event	Total Rainfall (mm)	Manning's n					Hydraulic Conductivity (m/day) ^[a]		Initial Soil Moisture Adjustment Ratio		Total Runoff (mm)		Peak Discharge (m ³ /s)	
		Stream	Forest	Grass/Alfalfa	Corn	Farmstead	High SMA	Low SMA	Stony	Silt Loam	Obs.	Pre.	Obs.	Pre.
2 July 94	24.02	0.03	0.15	0.14	0.17	0.09	1.20	0.80	1.066	1.072	1.72	1.64	0.234	0.235
22 July 94	24.76	0.02	0.26	0.20	0.23	0.12	2.00	0.80	0.520	0.560	1.17	1.00	0.236	0.230
18 Aug 94	22.62	0.04	0.20	0.14	0.17	0.09	1.20	0.80	0.610	0.690	5.99	5.54	0.276	0.267
Mean	23.80	0.03	0.20	0.16	0.19	0.10	1.47	0.80	0.732	0.774	2.96	2.73	0.249	0.244

^[a] SMA = Soil Moisture Area.

To simplify the calibration, the adjustment of initial soil moisture conditions was accomplished by categorizing the watershed's 11 soil types into 2 groups: stony and silt loam. A constant initial soil moisture adjustment factor was multiplied by the digital numbers of Frankenberger's soil moisture distribution map. The factor ranged from 0.520 for stony soils during the 22 July storm to 1.072 for silt loam soils during the 2 July storm, as shown in table 1. To apply Manning's equation in this study, the pond in the middle of the watershed was simply treated as a stream having very gentle slopes.

Figure 7 shows the observed versus predicted stream flow at the watershed outlet for the 2 July storm. The predicted runoff agreed well with the observed values, but the total runoff was underestimated for the three events, as summarized in table 1. Predicted runoff decreased rapidly at the falling limb for the 22 July and 18 August storms, but it decreased slowly at the baseflow recession for all storm events. This error may be caused by the scale-based parameterization of grid element processes with the undefined complexity of local heterogeneity and simplification of subsurface flow representation in the model. Preferential flow through macropores in the soil can contribute to stream flow as a subsurface lateral flow. Other sources of error may arise from the uncertainty of initial soil moisture condition and lumped parameters within each 10 m × 10 m grid element.

Sensitivity Analysis

To examine the effect of model parameters on simulation output, sensitivity analysis was conducted for the 2 July storm. The calibrated parameters [Manning's roughness coefficients (MRC), hydraulic conductivity (HC), and initial soil moisture adjustment ratio (ISMAR)] from table 1 were used as base values. Figure 8 shows the simulated stream flow at the watershed outlet with varying values of a target param-

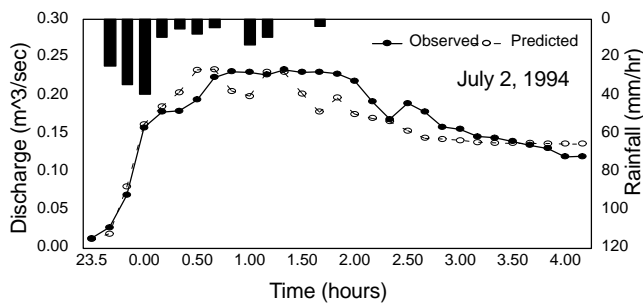


Figure 7. Comparison of predicted and observed stream flow for the 2 July storm.

eter, while keeping other parameters at the base value. The values in the legends are the multiplication ratios for the corresponding parameters.

Initial soil moisture distribution before a storm event (fig. 8C) proved to be the most sensitive parameter affecting the magnitude of peak discharge and total runoff within the capacity of soil moisture. The peak discharges for 0.9, 1.0, 1.05, 1.10, and 1.25 ISMAR were 0.170, 0.235, 0.828, 0.993, and 1.019 m³/sec, and the total runoff was 0.67, 1.64, 5.35, 6.09, and 6.29 mm, respectively. Manning's roughness coefficients for stream, forest, and grass/alfalfa were the second most sensitive parameters. The time of peak discharge moved from 0:40 hr to 1:24 hr as MRC of stream increased (fig. 8A). The peak discharges for 0.5, 0.75, 1.0, 1.5, and 2.0 MRC were 0.322, 0.268, 0.235, 0.262, and 0.263 m³/sec, and the total runoff was 1.70, 1.63, 1.64, 1.55, and 1.52 mm, respectively.

MRC for forest and grass/alfalfa affected the magnitude of peak discharge and total runoff the most. The time of peak discharge moved from 1:04 hr to 0:24 hr as MRC of forest increased. The peak discharges for 0.5, 0.75, 1.0, 1.5, and 2.0 MRC of forest were 0.363, 0.275, 0.235, 0.241, and 0.237 m³/sec, and the total runoff was 2.20, 1.81, 1.64, 1.54, and 1.42 mm, respectively. The discharge decreased as MRC for forest increased. The peak discharges for 0.5, 0.75, 1.0, 1.5, and 2.0 MRC of grass/alfalfa were 0.236, 0.225, 0.235, 0.300, and 0.337 m³/sec, and the total runoff was 1.76, 1.64, 1.64, 1.83, and 1.96 mm, respectively.

Note that the discharge increased as MRC for grass/alfalfa increased. Because this area is near the stream and has high initial soil moisture contents, the condition of overland flow is reached rapidly and drained to the stream without causing a time lag. MRC for corn and farmstead also affected the shape of the hydrograph depending on the areal portion of watershed.

Saturated hydraulic conductivity had little effect compared with other parameters (fig. 8B). This is due to the time scale of a storm event. Subsurface lateral flow should be a key component for long-term soil moisture routing in the water balance, but not for short-term storm runoff simulation. From the results of sensitivity analysis, we can conclude that ISMAR estimates water balance for the storm event to some extent, and then MRC and HC influence the peak time and rising and falling limbs of the hydrograph.

Model Verification

The model was verified using the average value of calibrated parameters from table 1 (except the initial soil moisture adjustment factor, which differs for each

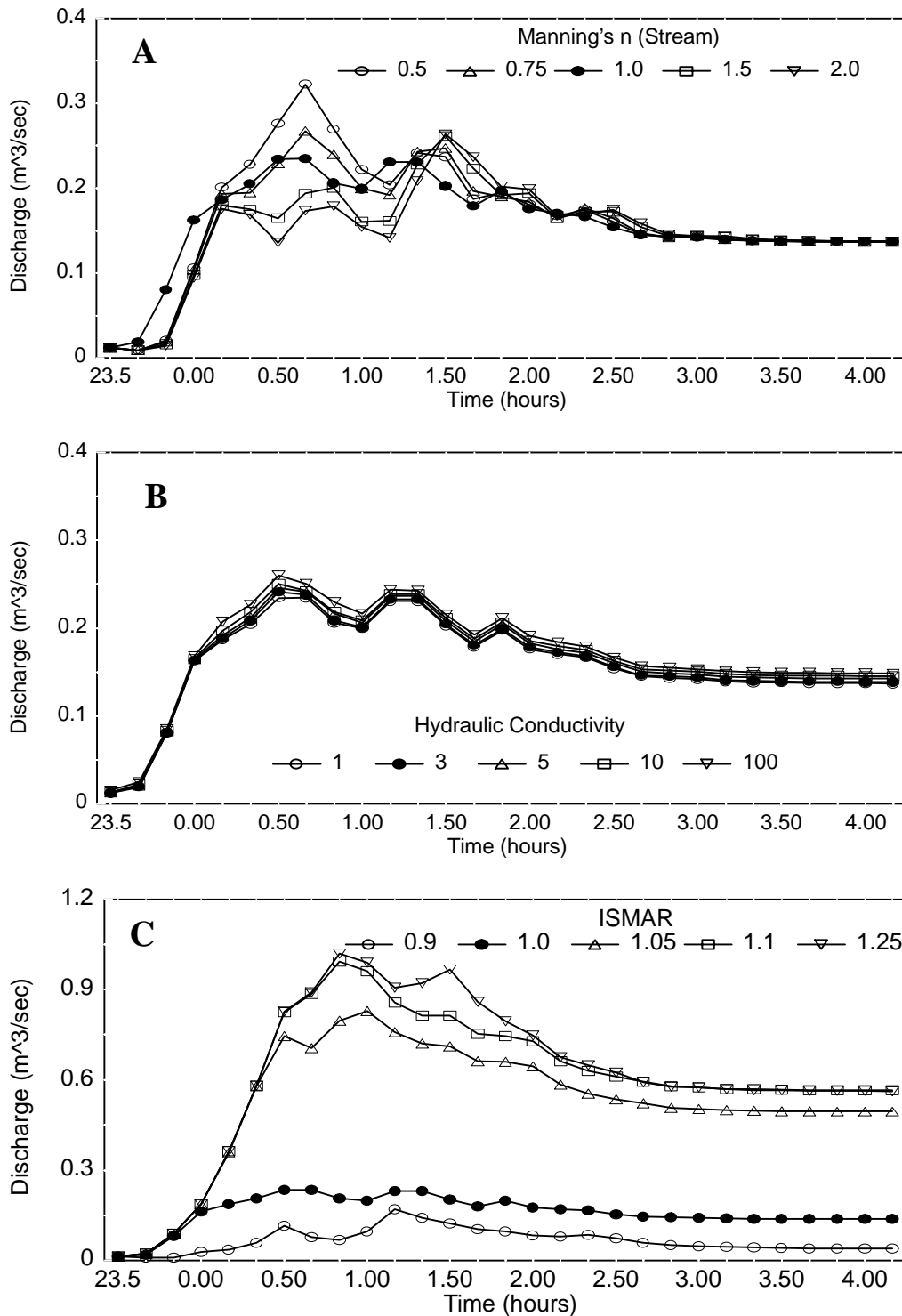


Figure 8. Parameter sensitivity of Manning's roughness coefficients, saturated hydraulic conductivity, and initial soil moisture distribution for the 2 July storm.

storm-event/soil-group combination) to predict stream flows at the watershed outlet for three other summer storms (14 August, 17 August, and 21 August, 1994). The maximum intensity and duration of the 14 August, 17 August, and 21 August storms were 35.3 mm/hr and 9.17 hours, 8.2 mm/hr and 5.33 hours, and 40.1 mm/hr and 2.0 hours, respectively. The adjustment factor for initial soil moisture ranged from 1.066 for stony soil during the 21 August storm, to 1.230 for silt loam soil during the 14 August storm. The predicted out-

let stream flows for the three storms were compared with observed values. Figure 9 shows the observed versus predicted stream flow at the watershed outlet for the 14 August storm. A summary of model verification is given in table 2. The average Nash-Sutcliffe efficiency R^2 (Nash and Sutcliffe, 1970) for the model was 0.72. Despite the verification of the model, many sources of uncertainty exist in the predictions of the variable source area storm runoff model. Beven and Binley (1992) listed other potential sources of error in

hydrologic modeling, such as deficiency of model structure, input data or boundary condition errors, and errors associated with measurements used in model calibration.

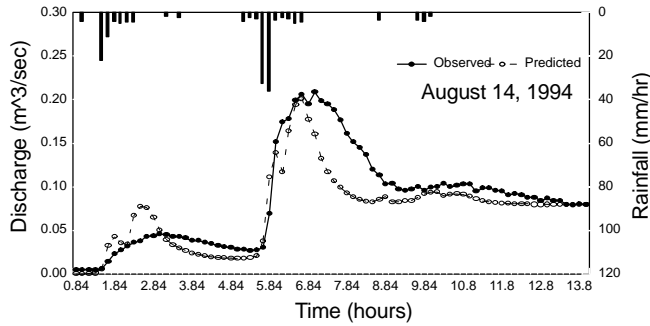


Figure 9. Comparison of predicted and observed stream flow for the 14 August storm.

Table 2. Summary of model verification.

Storm Event	Total Rainfall (mm)	Initial Soil Moisture Adjustment Ratio		Total Runoff (mm)		Peak Discharge (m ³ /s)		Nash Sutcliffe Efficiency R ²
		Silt		Obs.	Pre.	Obs.	Pre.	
		Stony	Loam					
14 Aug	25.80	1.180	1.230	2.30	1.94	0.209	0.201	0.754
17 Aug	17.68	1.071	1.076	2.04	1.83	0.172	0.186	0.742
21 Aug	14.64	1.066	1.072	3.18	2.90	0.256	0.242	0.653

TEMPORAL VARIATION AND SPATIAL DISTRIBUTION OF SATURATION OVERLAND FLOW

Knowing only the stream flow at the watershed outlet, we cannot determine where the overland flow originated and how much water each source area contributed. GIS can be used to simulate this information. This is important in investigating the loss of soil due to erosion and the transport of non-point source pollutants.

Figure 10 and figure 11 show the predicted temporal and spatial distribution of saturated overland flow discharges and flow depths for the 2 July storm. After the storm started at 23:24 hr, the overland flow areas initially occurred around the areas of the main stream that formed saturated areas. These areas had mild slopes, shallow soil depths, and higher initial soil moisture content than other areas. Topographic convergence caused more lateral inflow than outflow. Soils in these areas are composed of Norchip silt loam (No), Oteora channery silt loam (Oe), Torull-Gretor complex (Te), and Willowemoc channery silt loam (Wm), as shown in figure 5. Soil moisture contents in these areas before the storm (fig. 12) were originally over 0.4 cm³/cm³, while the other areas were under 0.4 cm³/cm³. The source area for overland flow increased from the start of rainfall until 23:54 hr and decreased gradually after that time. However, the peak flow was reached at 0:40 hr, as shown in figure 7. This shows that the overland/subsurface flows delayed the transport of water to the watershed outlet, causing a time lag. The other storm events showed results similar to the 2 July storm event.

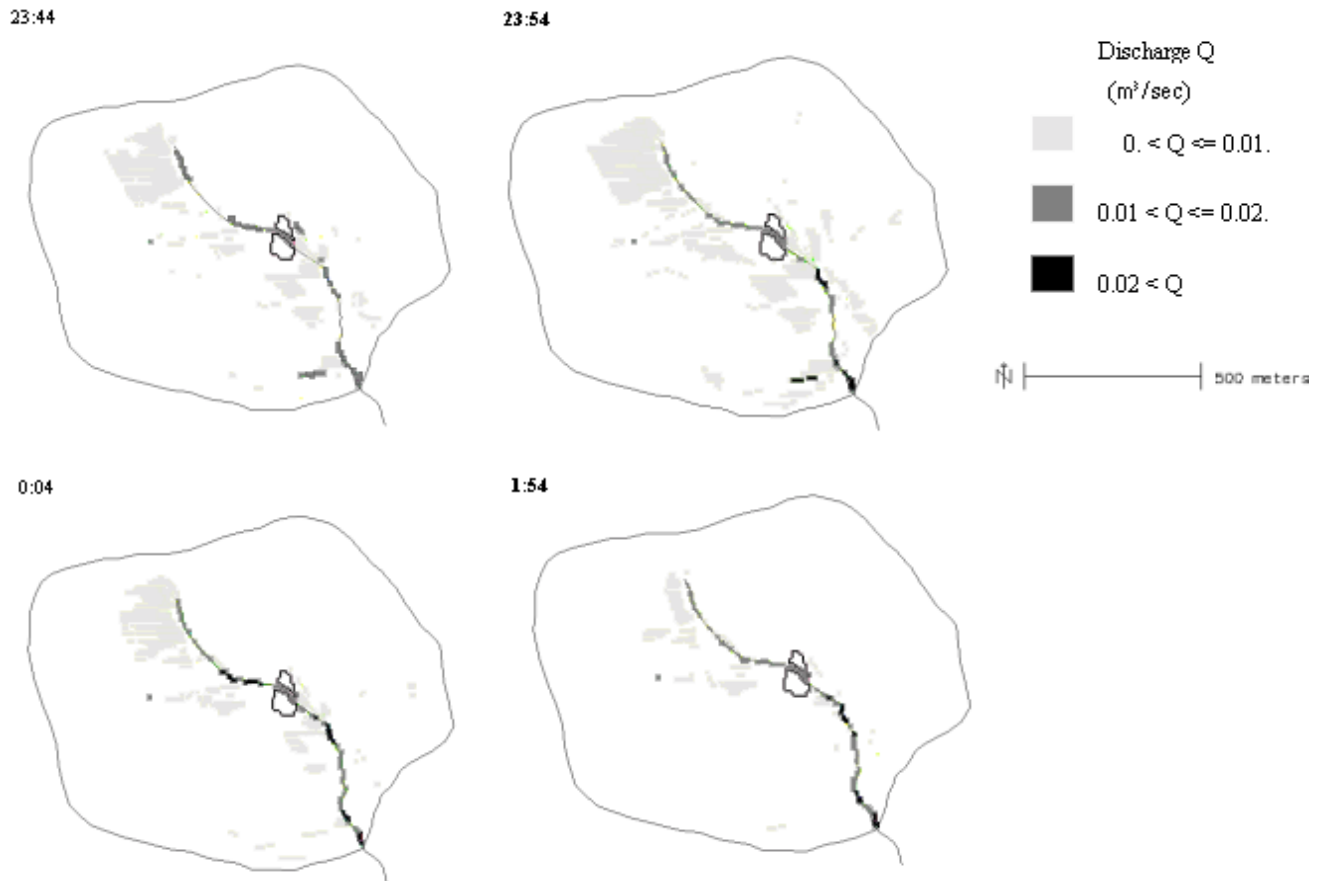


Figure 10. Temporal variation and spatial distribution of overland flow discharge (2 July 1994).

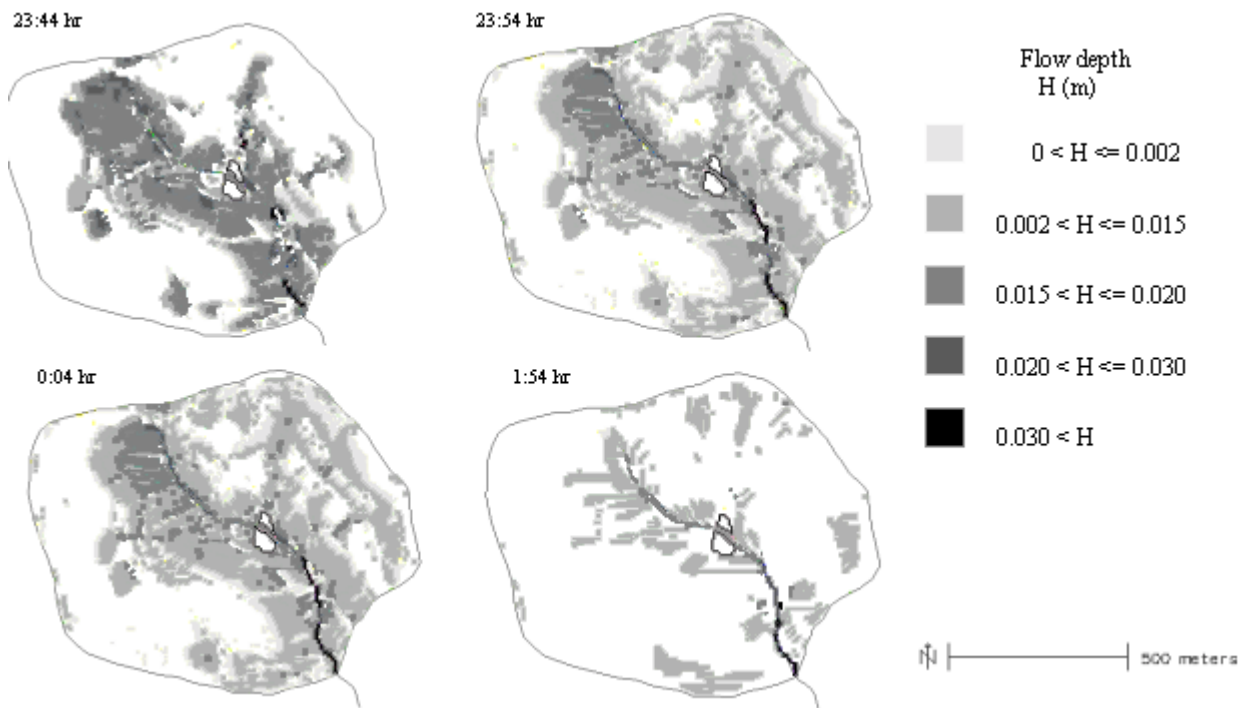


Figure 11. Temporal variation and spatial distribution of overland flow depth (2 July 1994).

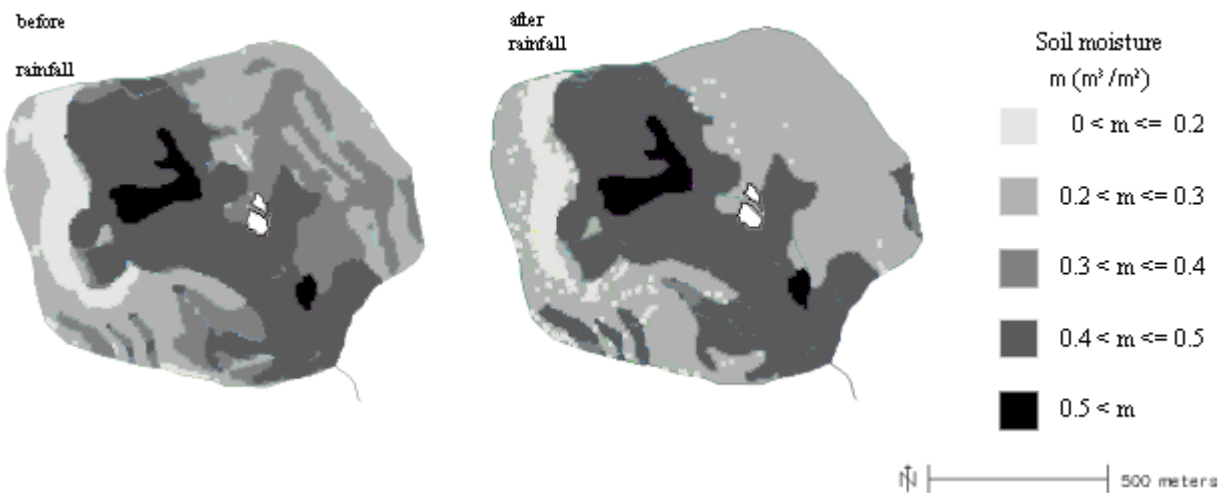


Figure 12. Spatial distribution of soil moisture before and after rainfall (2 July 1994).

SPATIAL EFFECT OF CHANGING GRID ELEMENT SIZE

Quinn et al. (1995) described the importance of grid resolution for the validation of spatial model prediction. They discussed the effect of the grid element size on the TOPMODEL (Beven and Kirkby, 1979) parameter, $\ln(a/\tan\beta)$ and model results. Refsgaard (1997) suggested the methodologies for the validation of new distributed models. He mentioned that multi-site runoff, soil moisture, or groundwater heads in a watershed should be measured and compared with the simulated ones for successful model validation. Even though this study did not sufficiently fulfill the distributed model's verification requirements in the manner of spatial verification, temporal calibration and verification with six storm events was performed by grouping

and adjusting saturated hydraulic conductivity and initial soil moisture content.

A spatial test of the model behavior by changing grid element size to 20, 30, and 40 m was conducted. In spatial aggregation, the values of the grid elements for continuous data, such as digital elevation models (DEMs) and three soil parameters, were averaged, while the most common value of the grid elements was selected for categorical data, such as soil, land use, and stream. New DEMs for 10, 20, 30, and 40 m grid elements are shown in figure 13A, B, C, and D, respectively. The slope distribution for each DEM is shown in figure 14A, B, C, and D. The average slopes were 8.11°, 7.81°, 7.76°, and 8.15°, respectively. The results show the deterioration of slope distribution and the losses of boundary

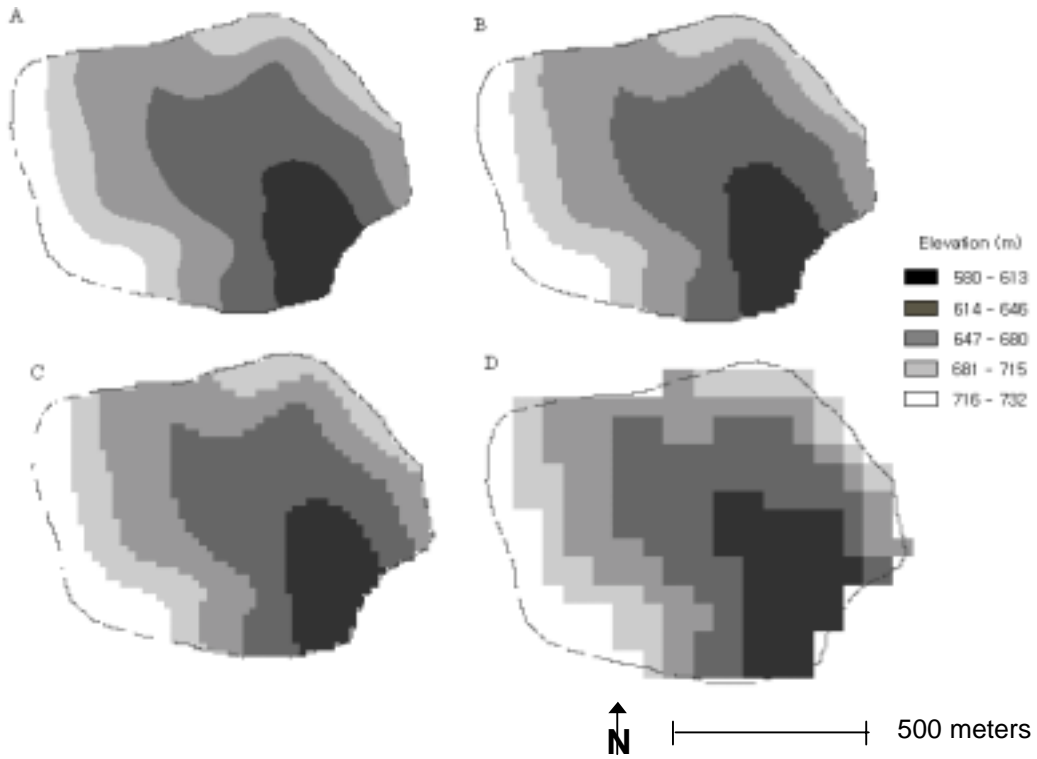


Figure 13. New DEMs for grid element size: (A) 10 m, (B) 20 m, (C) 30 m, and (D) 40 m.

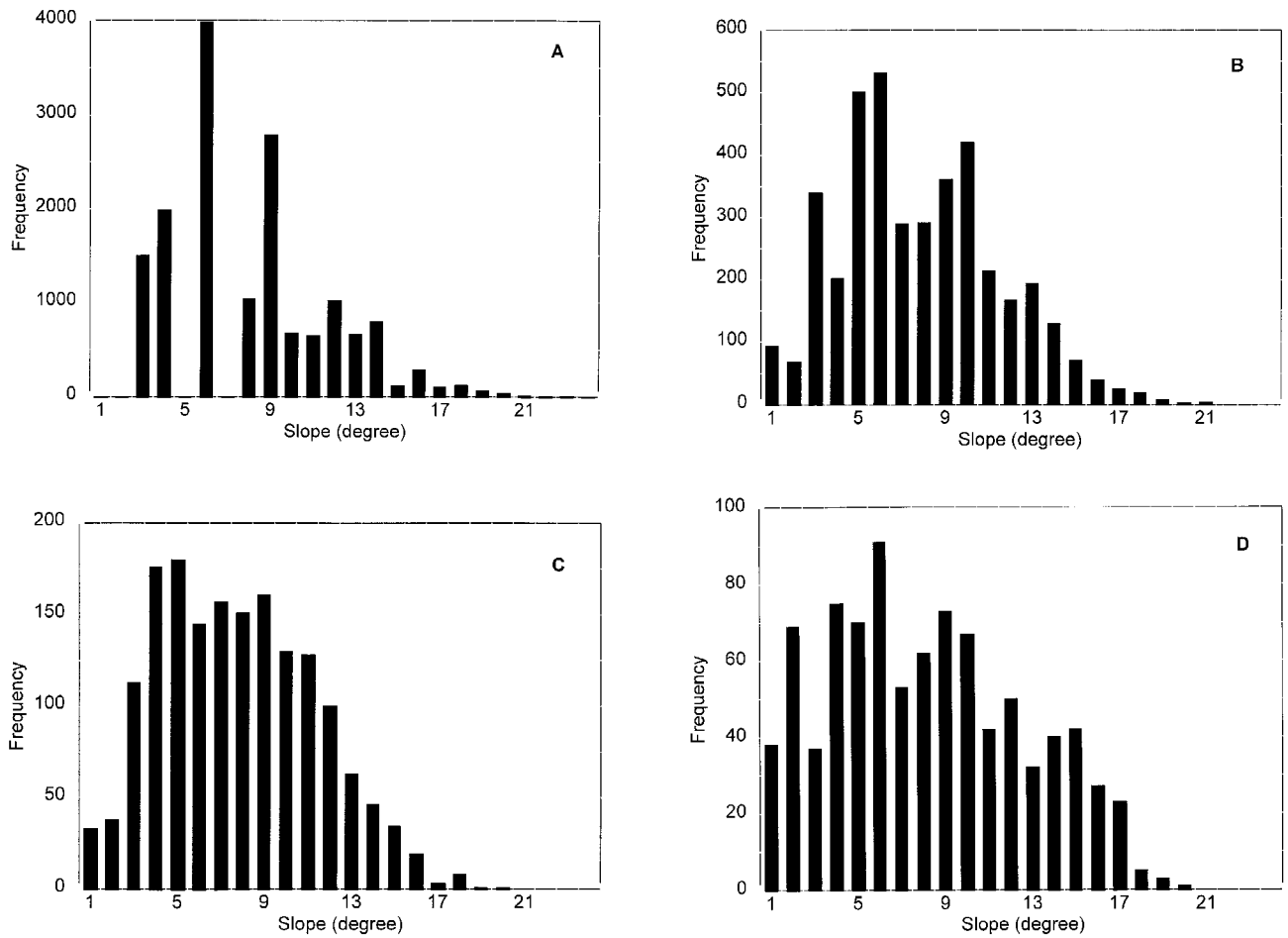


Figure 14. Slope distribution for each DEM: (A) 10 m, (B) 20 m, (C) 30 m, and (D) 40 m.

information with increasing grid element size. Recently, Kuo et al. (1999) suggested a new spatial aggregation method for border cells to conserve information inside the true boundary by considering the proportion of the border cell that is within the watershed. Model errors introduced by aggregation of spatial data may be reduced if the method by Kuo et al. (1999) is adopted. Because this study is not focused on the scaling effect toward macroscale hydrological modeling, the adjustment for border cells was not included.

Two parameters (saturated hydraulic conductivity and initial soil moisture adjustment ratio) were adjusted to fit to the observed flow while other parameters remain unchanged. This is because the smoothed slope from areal averaging clearly affects the subsurface flow velocity, and as described earlier in the model calibration section, the change in initial soil moisture distribution also affects the model result. Figure 15 shows the effect of changing grid element size on the prediction of 2 July stream flow at the watershed outlet. The calibrated saturated hydraulic conductivities for 20, 30, and 40 m grid elements were 580, 500, and 300 times greater than that for 10 m grid elements. The initial soil moisture adjustment ratios in stony and silt loam soils for 20, 30 and 40 m grid elements were calibrated as 0.951 and 0.958, 0.966 and 0.972, and 1.266 and 1.272, respectively. The need for soil moisture-related parameter adjustment can be explained by the fact that larger cells require higher initial soil moisture to account for subsurface flow.

Figure 16 shows the spatial effect of changing grid element size on the flow depth distribution for the 2 July storm at 0:40 hr. The overland flow areas for 20 and 30 m grid elements occurred just around the areas of the main stream, while those for 10 m grid elements occurred over the entire watershed. This is because the increased subsurface flow velocity cannot afford to produce the saturated overland flow in upland areas. The well-drained flow reaches the areas that

have mild slope and higher initial soil moisture content, and this forms the saturated overland flow. The 40 m grid element did not give a reasonable result, as shown in figure 15 and figure 16D. The source areas were randomly distributed in the watershed. From this result, we may deduce that the surface runoff that occurred in the grid elements could not be drained properly because of the smoother slope. The saturated hydraulic conductivity and the initial soil moisture condition exceeded the limit in controlling the water balance of the grid element. The adjustment of Manning's roughness coefficients for overland areas could improve the simulation result, but the calibrated values might be unrealistic to accept in a reasonable manner.

CONCLUSION

A grid-based storm runoff model was developed. This model generates the flow depth, discharge, soil moisture of subsurface flow, and saturated overland flow on a variable source area with shallow soil depths. The model uses regular gridded ASCII-formatted data from GRASS to predict the temporal variation and spatial distribution of saturation overland flow areas.

The model was tested in a small watershed located in the Northern Catskill region of New York State using GIS data with 10 m × 10 m grid size. The most sensitive parameter was the initial soil moisture distribution affecting the water balance for the storm event. The second most sensitive parameter was Manning's roughness coefficients for overland areas and streams affecting peak time and the ascending and descending phase of the hydrograph. For model calibration and verification, the observed stream flows measured at the watershed outlet were compared with values predicted by the model. The initial soil moisture conditions

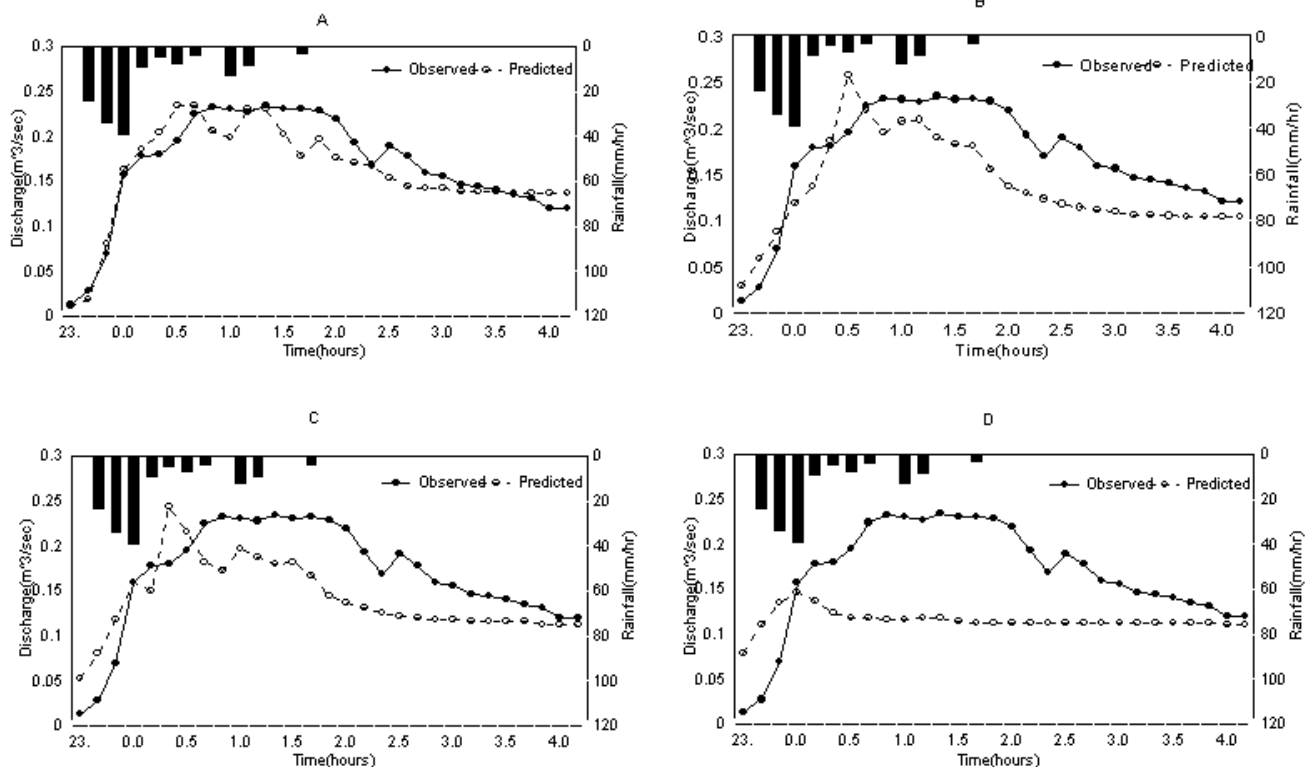


Figure 15. Effect of changing grid element size for predicting stream flow: (A) 10 m, (B) 20 m, (C) 30 m, and (D) 40 m (2 July 1994).

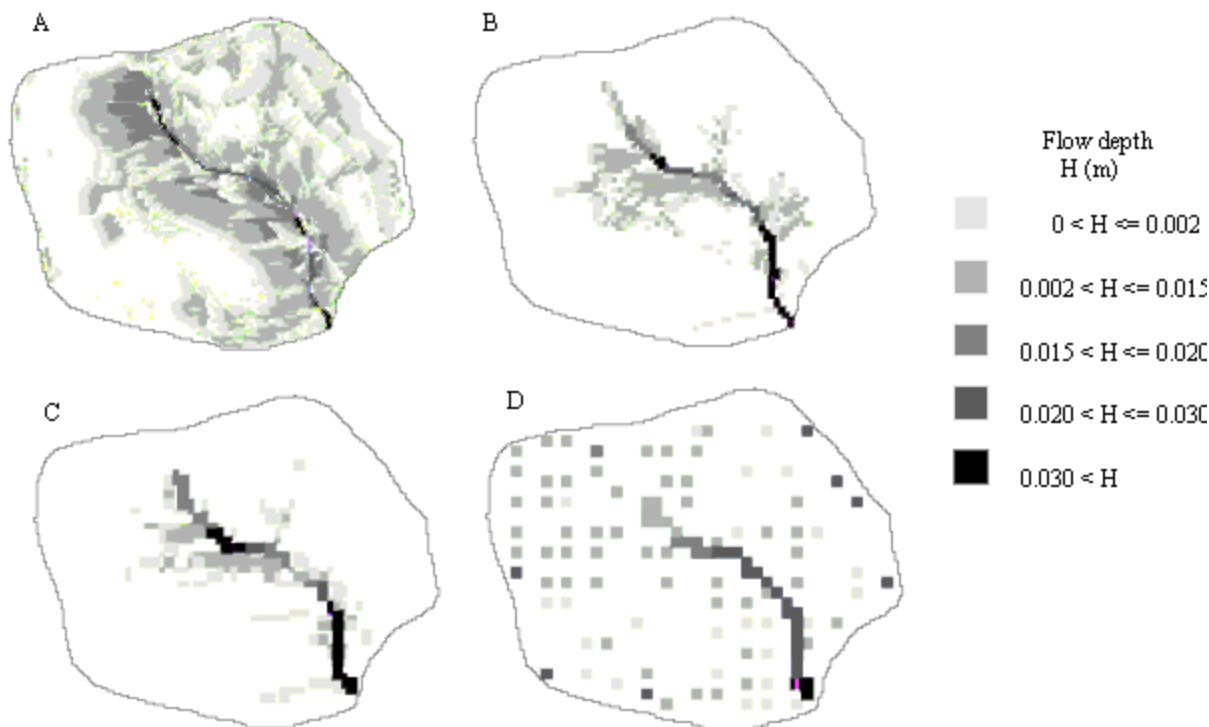


Figure 16. Spatial effect of changing grid element size for the 2 July storm at 0:40 hr represented by overland flow depth: (A) 10 m, (B) 20 m, (C) 30 m, and (D) 40 m.

for the storm events were adopted from the previous day's soil moisture distribution maps by Frankenberger's SMR model (Frankenberger, 1996). These were recalibrated by introducing adjustment factors for two soil types (stony and silt loam). The spatial distributions of saturated overland flow areas for several storm events were modeled and displayed with GRASS. The calculated overland flow areas occurred around the areas of the main stream that had high initial soil moisture contents. Temporal variation in those areas showed that the overland/subsurface flows attenuate and cause lag in stream flows. Finally, spatial testing was conducted by changing grid resolution to 20, 30, and 40 m. The model behavior was sensitive to DEM grid resolution. Increasing the grid element size deteriorated the slope distribution and lost the boundary information. This required parameter adjustment of saturated hydraulic conductivity and initial soil moisture adjustment ratio to obtain reasonable results.

ACKNOWLEDGEMENTS

The authors thank Dr. Jane Frankenberger of the Department of Agricultural and Biological Engineering, Purdue University, and Dr. Jan Boll of the Department of Biological and Agricultural Engineering, University of Idaho, for providing GIS and field data and for discussions that aided in the preparation of this article. Many thanks must be given to Dr. Mark Risse and the anonymous reviewers who improved earlier versions of this article. Thanks also go to Dr. Soon-Jin Hwang, who read proofs with religious care.

REFERENCES

Abbott, M. B., J. C. Bathurst, J. O. Cunge, P. E. O'Connell, and J. Rasmussen. 1986. An introduction to the European hydrological

system: Systeme Hydrologique Europeen (SHE). *J. Hydrology* 87(1): 45–59.

Allen, S. J. 1987. Digital hydrologic modeling methods for water resources engineering with application to the Broad Brook watershed. Ph.D. dissertation. The University of Connecticut, Storrs, Conn.

Beven, K. J., and A. Binley. 1992. The future of distributed models: Model calibration and uncertainty prediction. *Hydrol. Process.* 6(3): 279–298.

Beven, K. J., A. Calver, and E. M. Morris. 1987. *The Institute of Hydrology Distributed Model*. Report 98. Wallingford, U.K.: The Institute of Hydrology.

Beven, K. J., and M. J. Kirkby. 1979. A physically-based variable contributing area model of basin hydrology. *Hydrologic Sci. Bull.* 24(1): 43–69.

Brakensiek, D. L. 1967. Kinematic flood routing. *Trans. ASAE* 10(3): 340–343.

Dunne, T., and R. D. Black. 1970. Partial area contributions to storm runoff in a small New England watershed. *Water Resources Res.* 6(5): 1296–1311.

Famiglietti, J. S. 1992. Aggregation and scaling of spatially-variable hydrological process: Local catchment-scale and macroscale models of water and energy balance. Ph.D. dissertation. University of Maryland, College Park, Md.

Frankenberger, J. R. 1996. Identification of critical runoff generating areas using a variable source area model. Ph.D. dissertation. Cornell University, Ithaca, N.Y.

Frankenberger, J. R., E. S. Brooks, M. T. Walter, M. F. Walter, and T. S. Steenhuis. 1999. A GIS-based variable source area hydrology model. *Hydrol. Process.* 13(6): 805–822.

Goodchild, M. F. 1993. The state of GIS for environmental problem-solving. In *Environmental Modeling with GIS*, 8–15. M. F. Goodchild, B. O. Parks, and L. T. Steyaert, eds. New York, N.Y.: Oxford University Press.

Grayson, R. B., I. D. Moore, and T. A. McMahon. 1992. Physically based hydrological modeling. 1. A terrain-based model for investigative purposes. *Water Resources Res.* 28(10): 2659–2666.

- Grayson, R. B., G. Blöschl, and I. D. Moore. 1995. Distributed parameter hydrologic modeling using vector elevation data: THALES and TAPES-C. In *Computer Models of Watershed Hydrology*, 669–696. V. P. Singh, ed. Highlands Ranch, Colo.: Water Resources Publications.
- Hewlett, J. D., and W. L. Nutter. 1970. The varying source area of streamflow from upland basins. In *Proc. Symposium on Interdisciplinary Aspects of Watershed Management*, 65–83. Bozeman, Mont.: Montana State University. St. Joseph, Mich.: ASAE.
- Johnson, L. W., and R. D. Riess. 1982. Solution of nonlinear equations. In *Numerical Analysis*, 160–164. Boston, Mass.: Addison-Wesley.
- Kirkby, M. J. 1978. The hillslope hydrological cycle. In *Hillslope Hydrology*, 31. M. J. Kirkby, ed. Chichester, U.K.: John Wiley.
- Kuo, W.-L., T. S. Steenhuis, C. E. McCulloch, C. L. Mohler, D. A. Weinstein, S. D. DeGloria, and D. P. Swaney. 1999. Effect of grid size on runoff and soil moisture for a variable-source-area hydrology model. *Water Resources Res.* 35(11): 3419–3428.
- Moore, I. D., and G. J. Burch. 1986. Sediment transport capacity of sheet and rill flow: Application of unit stream power theory. *Water Resources Res.* 22(8): 1350–1360.
- Moore, I. D., and G. R. Foster. 1990. Hydraulics and overland flow. In *Process Studies in Hillslope Hydrology*, 215–254. M. G. Anderson and T. P. Burt, eds. New York, N.Y.: John Wiley.
- Nash, J. E., and J. V. Sutcliffe. 1970. River flow forecasting through conceptual models: Part I. A discussion of principles. *J. Hydrology* 10(3): 283–290.
- Nyerges, T. L. 1993. Understanding the scope of GIS: Its relationship to environmental modeling. In *Environmental Modeling with GIS*, 75–93. M. F. Goodchild, B. O. Parks, and L. T. Steyaert, eds. New York, N.Y.: Oxford University Press.
- Quinn, P. F., K. J. Beven, and R. Lamb. 1995. The $\ln(a/\tan\beta)$ index: How to calculate it and how to use it within the TOPMODEL framework. *Hydrol. Process.* 9(2): 161–182.

